Structural basis for recognition of anti-migraine drug lasmiditan by the serotonin receptor 5-HT_{1F}–G protein complex

Sijie Huang[1,2,3*], Peiyu Xu[1,2*], Yangxia Tan[1,2,3*], Chongzhao You[1,2], Yumu Zhang[1,2,3], Yi Jiang[1,2]†, and H. Eric Xu[1,2,3]†

[1]The CAS Key Laboratory of Receptor Research, Shanghai Institute of Materia Medica, Chinese Academy of Sciences, Shanghai 201203, China.

[2]University of Chinese Academy of Sciences, Beijing 100049, China.

[3]School of Life Science and Technology, ShanghaiTech University, 201210 Shanghai, China.

[*]These authors contributed equally: Sijie Huang, Peiyu Xu, Yangxia Tan

†Correspondence: yijiang@simm.ac.cn (Y.J.) and eric.xu@simm.ac.cn (H.E.X.)

Abstract

Migraine headache has become global pandemics and is the number one reason of work day loss. The most common drugs for anti-migraine are the triptan class of drugs that are agonists for serotonin receptors 5-HT_{1B} and 5-HT_{1D}. However, these drugs have side effects related to vasoconstriction that could have fatal consequences of ischemic heart disease and myocardial infarction. Lasmiditan is a new generation of anti-migraine drug that selectively binds to the serotonin receptor 5-HT_{1F} due to its advantage over the tripan class of anti-migraine drugs. Here we report the cryo-EM structure of the 5-HT_{1F} in complex with Lasmiditan and the inhibitory G protein heterotrimer. The structure reveals the mechanism of 5-HT_{1F}-selective activation by Lasmiditan and provides a template for rational design of anti-migraine drugs.

The serotonin 5-HT_1 receptor subtypes, including 5-HT_{1A}, 5-HT_{1B}, 5-HT_{1D}, 5-HT_{1e}, and 5-HT_{1F}, are G protein-coupled receptors (GPCRs) that respond to the endogenous neurotransmitter serotonin and couple preferentially to the $G_{i/o}$ family of G proteins[1]. Drugs targeting 5-HT_1 receptors are used to treat migraine, depression, and schizophrenia[2]. Clinical use of traditional anti-migraine drugs, triptans, caused side effects arising from therapeutic vasoconstrictive actions when targeting 5-$HT_{1B/1D}$ receptors[3]. The requirement of new anti-migraine drugs lacking vasoconstrictive effects led to the development of lasmiditan, a highly selective 5-HT_{1F} receptor agonist with minimizing on-target side effects[4].

Migraine is one of the most common diseases worldwide and, importantly, a major cause of lost work productivity[3]. The selective 5-$HT_{1B/D}$ agonists, triptans, are currently a first-line acute treatment of moderate-to-severe migraine attacks. Triptans bind mostly to 5-$HT_{1B/D}$ receptors within cerebral blood vessels, leading to vasoconstriction. Unfortunately, a large percentage of patients are not satisfied with current acute migraine treatments, because 5-$HT_{1B/D}$ receptors are also present on coronary and limb arteries and triptans may cause acute coronary syndromes in patients with or without cardiovascular disease[3,5].

Lasmiditan, a potent and selective agonist for the 5-HT_{1F} receptor, has recently been approved for acute migraine[6]. Lasmiditan lacks vasoconstriction effects and may be a safer and more effective option for patients refractory to treatment with triptans and for patients with cardiovascular disease[6]. Lasmiditan has a pyridinyl-piperidine scaffold, which is structurally different from the indole derivatives of triptans. In addition, Lasmiditan is able to penetrate the blood-brain barrier to act on receptor located in the brain, thus enhancing its action on receptor sites in central nervous system (CNS)[6]. To better understand the structural basis of lasmiditan for the 5-HT_{1F} selectivity and activation, we determined the structure of the 5-HT_{1F} in complex with lasmiditan and G_{i1} at a resolution of 3.4 Å by single-particle cryo-EM. The structure reveals the mechanism of 5-HT_{1F}-selective activation and provides a template for the rational design of anti-migraine drugs.

For single-particle cryo-EM structural studies, we prepared the lasmiditan-bound 5-HT_{1F}–G_i complex, which were met with technical challenges of low expression levels and unstable formation of the receptor-G protein complex. Despite these difficulties and after many attempts, we were able to prepare homogenous sample for cryo-EM analysis. The structure was determined at a global resolution of 3.4 Å (Supplementary information, Fig. S1). The lasmiditan-bound 5-HT_{1F}–G_i complex EM density maps are sufficiently clear to define the position of the 5-HT_{1F} receptor, the G_i heterotrimer, scFv16, and the bound ligand lasmiditan. The overall structure of 5-HT_{1F} consists of a canonical transmembrane domain (TMD) of seven transmembrane helices (TM1-7), a short intracellular loop 2 (ICL2) helix, and an amphipathic helix H8 (Fig. 1a, b). The active 5-HT_{1F} receptor shares a similar overall conformation with other active 5-HT_1 receptors[7], while a complete backbone structure for ECL2 is visible, which is partly missing in other 5-HT_1 structures due to the flexibility. The cryo-EM map includes well-defined features for amino acids forming the agonist-binding pocket and clear density for lasmiditan in 5-HT_{1F} (Fig. 1b). We found that negatively charged amino acids in the ligand binding pocket of 5-HT_{1F} are primarily responsible for the affinity of lasmiditan (Fig. 1c, d). In the orthosteric binding pocket (OBP), the primary amine on methylpiperidine group of lasmiditan forms a canonical charge interaction with $D103^{3x32}$ of 5-HT_{1F} (Fig. 1d), which simultaneously forms a hydrogen bond with $Y337^{7x42}$, supporting a stable interaction between the ligand and the receptor (Fig. 1d). Mutational studies showed these residues are critical for lasmiditan binding (Supplementary information, Fig. S2). The interactions from D^{3x32} of the receptor to the primary amine of agonists and the supportive Y^{7x42} are conserved in aminergic GPCRs[8]. In addition, the methylpiperidine group of lasmiditan forms hydrophobic interactions with $F309^{6x51}$ in TM6 of 5-HT_{1F} (Fig. 1d), mutation in $F309^{6x51}$ cause a nearly 100-fold reduction of lasmiditan affinity (Supplementary information, Fig. S2). Meanwhile, the aromatic pyridine scaffold of lasmiditan is sandwiched between $I104^{3x33}$ and $F310^{6x52}$, forming a hydrophobic interaction core (Fig. 1d). $F310^{6x52}$A mutation simultaneously eliminated 5-HT_{1F}-G protein coupling signals and lasmiditan affinity, and $I104^{3x33}$ A mutation also cause a nearly 60-fold reduction of lasmiditan affinity, suggesting that these hydrophobic interactions are crucial for lasmiditan-induced 5-HT_{1F} activation (Supplementary information, Fig. S2). I^{3x33} of 5-HT_{1F} is 3.5 Å away from the aromatic ring of

lasmiditan, which provides a stronger hydrophobic interaction than V^{3x33} of 5-HT_{1A} and M^{3x33} of 5-HT_{1E}. In the extended binding pocket (EBP), the trifluorobenzene group of lasmiditan forms additional hydrophobic interactions with $I174^{ECL2}$ and $P158^{4x60}$, and forms hydrogen bonds with residue $E313^{6x55}$, $N317^{6x59}$, $T182^{5x40}$, and $H176^{ECL2}$ of 5-HT_{1F} (Fig. 1d). These structural observations are also confirmed by mutation experiments (Supplementary information, Fig. S2).

Lasmiditan is a new generation 5-HT receptor agonist with high affinity and selectivity for 5-HT_{1F} (Ki = 2 nM) over other serotonin receptors (Ki > 500 nM)[4], and this selectivity is also confirmed by our NanoBiT G-protein recruitment assays (Fig. 1e; Supplementary information, Fig. S3a). Comparison of the structure of 5-HT_{1F} bound to lasmiditan with other 5-HT_1 structures[7,9] uncovers the structural basis of selectivity for lasmiditan (Fig. 1f-h). Comparison of 5-HT_{1F} with 5-HT_{1B} shows that the ligand-receptor interaction are basically conserved in OBP, while differences in EBP, which are formed by TM4/5/6, and ECL2. For the TM4/5, the residues that interact with the trifluorobenzene group of lasmiditan in 5-HT_{1F} are highly conserved with 5-HT_{1B} (Fig. 1f). However, the conformation of TM4/5 shows significant changes between 5-HT_{1F} and 5-HT_{1B}. On the extracellular side, TM4 shifts 3.6 Å, and TM5 shifts 2.8 Å for 5-HT_{1F} from those in 5-HT_{1B} (Fig. 1f). For the TM6, the E^{6x55} and N^{6x59} of 5-HT_{1F} form hydrogen bonds with lasmiditan, but the corresponding residues are S^{6x55} and P^{6x59} in 5-HT_{1B}, and they cannot provide the corresponding interactions. For the ECL2, including the region that interacts with lasmiditan shows different conformations between 5-HT_{1F} and 5-HT_{1B} (Fig. 1f).

5-HT_{1E} is the receptor with the highest homology to 5-HT_{1F}. The structure of 5-HT_{1E} we previously reported reveals the mechanism of the 5-$HT_{1E/1F}$ selective ligand BRL54443 for 5-HT_{1E}. Lasmiditan is only selective for 5-HT_{1F}, rather than for 5-HT_{1E}. Structural comparison of 5-HT_{1F} and 5-HT_{1E} provides an opportunity to uncover the mechanism of selectivity of lasmiditan on 5-HT_{1F}. Although 5-HT_{1F} and 5-HT_{1E} have relatively conserved residues for ligand binding both in OBP and EBP, the conformations of TM4, TM5, and ECL2 show significant differences. Among them, the extracellular end of TM4 shifted by 3.5 Å, TM5 shifted by 2.0 Å, and the backbone of ECL2 shows different conformarion (Fig.

1g). These changes are similar in comparison with 5-HT$_{1B}$ (Fig. 1f). We further compared the 5-HT$_{1F}$ structure with other 5-HT$_1$ subfamily receptors, the results showed that the conformation of the TM4-TM5-ECL2 region is relatively conserved in 5-HT$_{1A}$, 5-HT$_{1B}$, 5-HT$_{1D}$, and 5-HT$_{1E}$, but not for 5-HT$_{1F}$ (Fig. 1h; Supplementary information, Fig. S3b-d). To confirm the roles of ECL2 on ligand selectivity, we replaced the ECL2 of 5-HT$_{1F}$ with that of other 5-HT$_1$ receptors and tested the receptor activation. The result shows that the lasmiditan induced activation was significantly affected (Supplementary information, Fig. S3e). The importance of EPB for lasmiditan binding and the different shape of EBP of 5-HT$_{1F}$ from other 5-HT receptors determines the high selectivity of lasmiditan on 5-HT$_{1F}$.

The lasmiditan induces activation for 5-HT$_{1F}$ undergoing a canonical conformational rearrangement. Comparing to the inactive state 5-HT$_{1B}$[10], lasmiditan triggers the toggle switch residue W^{6x48} of 5-HT$_{1F}$ downward movement, then induces the conformational changes in PIF, DRY, and NPxxY motifs (Supplementary information, Fig. S4a-e). These conformational changes further cause an 8 Å outward movement of TM6, which allows the α5 helix of Gα_{i1} insert into the intracellular cavity formed by the receptor TMD bundle, a hallmark of GPCR activation (Supplementary information, Fig. S4f). Structural comparison of the G$_i$-coupled 5-HT$_{1F}$ with the G$_o$-coupled 5-HT$_{1B}$ complexes[9] reveals differences in G-protein coupling (Supplementary information, Fig. S4g, h). Although the conformation of the main interfaces between receptor and G-protein are similar, the G-protein conformation shows observable changes. The main body of the Ras-like domain shares a similar conformation, while the N-terminus of αN shift 9.4 Å and the last residue of α5 shift 2.4 Å between G$_i$ and G$_o$ (Supplementary information, Fig. S4g). Comparing the 5-HT$_{1F}$–G$_i$ complex with other 5-HT$_1$–G$_{i/o}$ complex structures[7,9], we found that the αN of 5-HT$_{1F}$ bound G$_i$ shifts away from other 5-HT$_1$ receptors bound G$_{i/o}$, which suggests that the coupling of 5-HT$_{1F}$ to G$_i$ protein is unique from other 5-HT$_1$ receptors (Fig. 1i).

In summary, in this paper, we report the cryo-EM structure of the 5-HT$_{1F}$–Gi complex bound to a highly selective anti-migraine drug lasmiditan. The structure reveals the binding mode of lasmiditan in 5-HT$_{1F}$. Comparison of our structure with the previously reported 5-HT$_1$ structures[9] provide the basis of the

selectivity for lasmiditan to 5-HT_{1F}. The determination for selectivity mainly attributes to the interaction between the trifluorobenzene group of lasmiditan and the specific extended binding pocket (EBP) of 5-HT_{1F}. Furthermore, our structure reveals a conserved mechanism for activation of 5-HT_{1F} and the unique G protein coupling conformation from that in the 5-HT_1–G-protein structures[7,9]. Together, these results provide a rational template for design of new generation of anti-migraine drugs that selectively target 5-HT_{1F}, therefore avoiding the main disadvantage of cardiovascular side effects associated with the triptan class of anti-migraine drugs.

Fig. 1 Structure of lasmiditan–5-HT_{1F}–G_{i1} complex. a Cryo-EM map of the 5-HT_{1F}–G_i complex. **b** Structural model of the 5-HT_{1F}–G_i complex. The ligand model is shown on left side of the complex with surrounding density map. **c** Electrostatic surface representation of lasmiditan binding pocket of 5-HT_{1F}. **d** The binding mode of lasmiditan in the ligand binding pocket of 5-HT_{1F}. **e** G_i recruitment assay using NanoBiT for wild type 5-HT_{1A}, 5-HT_{1B},5-HT_{1D}, 5-HT_{1E}, and 5-HT_{1F} induced by serotonin, donitriptan and lasmiditan. **f** Structural comparison of lasmiditan-bound 5-HT_{1F} with donitriptan-bound 5-HT_{1B} (PDB code: 6G79). **g** Structural comparison of lasmiditan-bound 5-HT_{1F} with BRL54443-bound 5-HT_{1E} (PDB code: 7E33). **h** Structure comparison focus on extracellular end of TM4 (left) and TM5 (right) among 5-HT_{1A} (red, PDB code: 7E2Y), 5-HT_{1B} (tan, PDB code: 6G79), 5-HT_{1D} (yellow, PDB code: 7E32), 5-HT_{1E} (blue, PDB code: 7E33) and 5-HT_{1F} (green). **i** Comparison of the G_α conformation among the structures of $G_{i/o}$ coupled 5-HT_{1A} (red, PDB code: 7E2Y), 5-HT_{1B} (tan, PDB code: 6G79), 5-HT_{1D} (yellow, PDB code: 7E32), 5-HT_{1E} (blue, PDB code: 7E33) and 5-HT_{1F} (green).

Data availability

The corresponding coordinates and cryo-EM density map have been deposited in the Protein Data Bank (http://www.rcsb.org/pdb) with code 7EXD, and in EMDB (http://www.ebi.ac.uk/pdbe/emdb/) with code EMD-31371.

Acknowledgements

The cryo-EM data were collected at the Cryo-Electron Microscopy Research Center, Shanghai Institute of Materia Medica, Chinese Academy of Sciences (Shanghai, China). This work was partially supported by the Ministry of Science and Technology (China) grant (2018YFA0507002 to H.E.X.); CAS Strategic Priority Research Program (XDB37030103 to H.E.X.); Shanghai Municipal Science and Technology Major Project (2019SHZDZX02 to H.E.X.); the National Natural Science Foundation (31770796 to Y.J.); National Science & Technology Major Project "Key New Drug Creation and Manufacturing Program" (2018ZX09711002-002-002 to Y.J.).

Author contributions

S.H. and P.X. designed the expression constructs, purified the complexes, prepared samples for negative stain and data collection toward the structures, performed functional assay, prepared the figures and manuscript draft. P.X. evaluated the specimen by negative-stain EM, screened the cryo-EM conditions, prepared the cryo-EM grids, collected cryo-EM images, built the model, and refined the structures. Y.T., C.Y., and Y.Z. participated in the NanoBiT G-protein recruitment assays. Y.J. participated in the supervision of S.H., P.X., Y.T., C.Y., and Y.Z. and analyzed the structures, edited the manuscript. H.E.X. conceived and supervised the project, analyzed the structures, and wrote the manuscript with inputs from all authors.

Competing interests: The authors declare no competing interests.

References

1 McCorvy, J. D. & Roth, B. L. Structure and function of serotonin G protein-coupled receptors. *Pharmacol*

Therapeut **150**, 129-142, doi:10.1016/j.pharmthera.2015.01.009 (2015).

2 Pytliak, M., Vargova, V., Mechirova, V. & Felsoci, M. Serotonin receptors - from molecular biology to clinical applications. *Physiol Res* **60**, 15-25, doi:10.33549/physiolres.931903 (2011).

3 Negro, A., Koverech, A. & Martelletti, P. Serotonin receptor agonists in the acute treatment of migraine: a review on their therapeutic potential. *J Pain Res* **11**, 515-526, doi:10.2147/JPR.S132833 (2018).

4 Nelson, D. L. *et al.* Preclinical pharmacological profile of the selective 5-HT1F receptor agonist lasmiditan. *Cephalalgia* **30**, 1159-1169, doi:10.1177/0333102410370873 (2010).

5 Weder, C. R. & Schneemann, M. Triptans and troponin: a case report. *Orphanet J Rare Dis* **4**, 15, doi:10.1186/1750-1172-4-15 (2009).

6 Clemow, D. B. *et al.* Lasmiditan mechanism of action - review of a selective 5-HT1F agonist. *J Headache Pain* **21**, 71, doi:10.1186/s10194-020-01132-3 (2020).

7 Xu, P. *et al.* Structural insights into the lipid and ligand regulation of serotonin receptors. *Nature*, 1-5 (2021).

8 Michino, M. *et al.* What can crystal structures of aminergic receptors tell us about designing subtype-selective ligands? *Pharmacol Rev* **67**, 198-213, doi:10.1124/pr.114.009944 (2015).

9 Garcia-Nafria, J., Nehme, R., Edwards, P. C. & Tate, C. G. Cryo-EM structure of the serotonin 5-HT1B receptor coupled to heterotrimeric Go. *Nature* **558**, 620-623, doi:10.1038/s41586-018-0241-9 (2018).

10 Yin, W. *et al.* Crystal structure of the human 5-HT1B serotonin receptor bound to an inverse agonist. *Cell Discov* **4**, 12, doi:10.1038/s41421-018-0009-2 (2018).

Supplementary information

Supplementary information, Figure S1

Fig. S1 Sample preparation and cryo-EM of the 5-HT_{1F}–G_{i1} complexes. **a** Analytical size-exclusion chromatography of the purified complex and SDS-PAGE/Coomassie blue stain of the purified complex. **b**, **c** Representative cryo-EM image and 2D averages. **d** Flowchart of cryo-EM data analysis of the lasmiditan bound-5-HT_{1F}–G_i complex. **e** Euler angle distribution of particles used in the final reconstruction. **f** 'Gold-standard' Fourier shell correlation curves of the lasmiditan–5-HT_{1F}–G_i complex.

Supplementary information, Figure S2

Fig. S2 Mutagenesis data of lasmiditan mediate 5-HT_{1F} activation by NanoBiT Gi-protein-recruitment assay. **a** Dose response cuves of mutations on ligand-binding pocket. **b** Dose response cuves of mutations on G-protein interaction interface. **c** pEC_{50} of mutations on G-protein interaction interface and ECL2 chimeraic receptors. **d** pEC_{50} of mutations on ligand-binding pocket. Data are mean ± s.e.m. from at least three independent experiments performed in technical triplicate.

Supplementary information, Figure S3

Fig. S3 Selectivity of lasmiditan. a Dose response cuves and pEC50 of 5-HT, donitriptan, and lasmiditan induced activation of 5-HT_{1A}, 5-HT_{1B}, 5-HT_{1D}, 5-HT_{1E} and 5-HT_{1F}. b comparison of the ligand-binding pocket among the structures of $G_{i/o}$ coupled 5-HT_{1A} (red, PDB code: 7E2Y), 5-HT_{1B} (tan, PDB code: 6G79), 5-HT_{1D} (yellow, PDB code: 7E32), 5-HT_{1E} (blue, PDB code: 7E33) and 5-HT_{1F} (green). **c, d** Comparison of TM4-TM5-ECL2 region among 5-HT_1 sub-family receptors. c, extracellular view; d, side view. **e** The replacement of ECL2 of 5-HT_{1F} with other 5-HT_1 receptors affects the lasmiditan mediate activation. Data are mean ± s.e.m. from at least three independent experiments performed in technical triplicate.

Supplementary information, Figure S4

Fig. S4 Lasmiditan induced activation of 5-HT_{1F}. **a** Structural uperposition of active 5-HT_{1F} and inactive 5-HT_{1B} (PDB code: 5v54) complexes. **b-e** residues rearrangement of Toggle switch (**b**), PIF motif (**c**), DRY motif (**d**), and NPxxY motif (**e**). **f** The outwad movement of intracellular end of TM6. **g** Comparison of the 5-HT_{1F} bound $G\alpha_i$ conformation and 5-HT_{1B} bound $G\alpha_o$ conformation. The left arro indicates the movement of αN helix in $G\alpha_i$ structure relative to $G\alpha_o$ structure. The right arrow indicates the movement of the last amino acid in the Gα α5 helix in $G\alpha_i$ structure relative to $G\alpha_o$ structure. **i** Comparison of ICL2-G protein interactions in the 5-HT_{1F}–G_i and 5-HT_{1B}–mG_o structures.

Materials and methods

Constructs of 5-HT_{1F} and G_{i1} heterotrimer

The full-length gene sequences of wild type *human* 5-HT_{1F} receptors were subcloned into pFastbac vector using ClonExpress II One Step Cloning Kit (Vazyme Biotech Co.,Ltd). An N-terminal thermally stabilized BRIL[1] as a fusion protein to enhance receptor expression. N-terminal fusions of Flag tag and 8×His tag were used to facilitate protein purification. A dominant-negative $G\alpha_{i1}$ was generated by site-directed mutagenesis to incorporate mutations S47N, G203A, A326S, and E245A that improves the dominant-negative effect by weakening a salt bridge that helps to stabilize the interactions with the βγ subunits[2]. All the three G_i subunits, *human* DN_$G\alpha_{i1}$, wild type Gβ1, and Gγ2 were cloned into the pFastBac vector separately. A no-tag single-chain antibody scFv16[3] was cloned into pFastBac.

Insect cell expression

Human 5-HT_{1F}, DN$G\alpha_{i1}$, $G\beta_1$, $G\gamma_2$,and scFv16 were co-expressed in *Trichoplusia ni* Hi5 insect cells using the baculovirus method (Expression Systems). Cell cultures were grown in ESF 921 serum-free medium (Expression Systems) to a density of 2-3 million cells per ml and then infected with four separate baculoviruses at a suitable ratio. The culture was collected by centrifugation 48 h after infection and cell pellets were stored at -80°C.

Complex purification

The complex was purified as previously described[4]. In brief, cell pellets were thawed in 20 mM HEPES pH 7.4, 50 mM NaCl, 10 mM $MgCl_2$ supplemented with Protease Inhibitor Cocktail (Bimake). The 5-HT_{1F} complex formation was initiated by addition of 10 μM lasmiditan (TargetMol), apyrase (25 mU/ml, Sigma). The suspension was incubated for 1 h at room temperature and the complex was solubilized from the membrane using 0.5% (w/v) n-dodecyl-β-d-maltoside (DDM, Anatrace) and 0.1% (w/v) cholesteryl hemisuccinate (CHS, Anatrace) for 2 h at 4°C. Insoluble material was removed by centrifugation at 65,000 g for 30 min and the solubilized complex was immobilized by batch binding to Talon affinity resin. The resin was then packed and washed with 20 column volumes of 20 mM HEPES pH 7.4, 100 mM NaCl, 5 mM $MgCl_2$, 0.01% (w/v) LMNG, and 0.002% (w/v) CHS, 10 μM lasmiditan. Finally, the complex was eluted in buffer containing 300 mM imidazole and concentrated with an Amicon Ultra Centrifugal Filter (MWCO 100 kDa). Complex was subjected to size-exclusion chromatography on a Superdex 200 Increase 10/300 column (GE Healthcare) pre-equilibrated with 20 mM HEPES pH 7.4, 100 mM NaCl, 0.05% (w/v) digitonin, and 10 μM lasmiditan, to separate complex from contaminants. Eluted fractions consisting of receptor and G_i-protein complex were pooled and concentrated.

NanoBiT G-protein recruitment assay

Analysis of G-protein recruitment was performed by using a modified protocol of NanoBiT system (Promega) assay described previously[5]. Receptor-LgBiT, $G\alpha_{i1}$, SmBiT-fused $G\beta_1$, and $G\gamma_2$ were co-expressed in *Trichoplusia ni* Hi5 insect cells using the baculovirus method (Expression Systems). Cell cultures were grown in ESF 921 serum-free medium (Expression Systems) to a density of 2-3 million cells per ml and then infected with four separate baculoviruses at a suitable ratio. The culture was collected by centrifugation 48 h after infection and cell pellets were collected with PBS. The cell suspension was dispensed in a white 384-well plate at a volume of 40 μl per well and loaded with 5 μl of 90 μM coelenterazine diluted in the assay buffer. Test compounds (5 μl) were added and incubated for 3-5 min at room temperature before measurement. Luminescence counts were normalized to the initial

count and fold-change signals over vehicle treatment were used to show G-protein binding response.

Cryo-EM grid preparation and data collection

For the preparation of cryo-EM grids, 3 μL of the purified lasmiditan–5-HT_{1F}–G_i complex at concentration ~15 mg/ml were applied onto a glow-discharged holey carbon grid (Quantifoil R1.2/1.3 Au 300). Grids were plunge-frozen in liquid ethane using Vitrobot Mark IV (Thermo Fisher Scientific). Frozen grids were transferred to liquid nitrogen and stored for data acquisition. Cryo-EM imaging was performed on a Titan Krios at 300 kV using Gatan K3 Summit detector in the Cryo-Electron Microscopy Research Center, Shanghai Institute of Materia Medica, Chinese Academy of Sciences (Shanghai, China). The images were recorded at a dose rate of about 26.7 $e^-/Å^2/s$ with a defocus ranging from -1.2 to -2.2 μm. The total exposure time was 3 s and intermediate frames were recorded in 0.083 s intervals, resulting in a total of 36 frames per micrograph.

Image processing and map construction

Dose-fractionated image stacks were aligned using MotionCor2.1[6]. Contrast transfer function (CTF) parameters for each micrograph were estimated by Gctf[7]. Cryo-EM data processing was performed using RELION-3.1[8]. Automated particle picking yielded 4,075,443 particles that were subjected to reference-free 2D classification to discard poorly defined particles, producing 1,467,387 particles. The map of 5-HT_{1B}–miniG_o complex (EMDB-4358)[9] low-pass filtered to 60 Å was used as an initial reference model for 3 rounds of 3D classification. Two subsets show the high-quality receptor density was selected, producing 263,350 particles. The selected subsets was subsequently subjected to 3D refinement, CTF refinement, Bayesian polishing, and DeepEMhancer[10]. The final refinement generated a map with an indicated global resolution of 3.4 Å at a Fourier shell correlation of 0.143. Local resolution was determined using the 3DFSC package with half maps as input maps.

Model building and refinement

The cryo-EM structure of 5-HT_{1B}–mG_o complex (PDB code: 6G79) and the G_i protein model (PDB code: 6PT0) were used as the start for model rebuilding and refinement against the electron microscopy map. The model was docked into the electron microscopy density map using Chimera[11], followed by iterative manual adjustment and rebuilding in COOT[12] and ISOLDE[13]. Real space and reciprocal space refinements were performed using Phenix programs[14]. The model statistics were validated using MolProbity[15]. Structural figures were prepared in Chimerax[16].

References

1 Chun, E. *et al.* Fusion partner toolchest for the stabilization and crystallization of G protein-coupled receptors. *Structure* **20**, 967-976, doi:10.1016/j.str.2012.04.010 (2012).

2 Liang, Y. L. *et al.* Dominant Negative G Proteins Enhance Formation and Purification of Agonist-GPCR-G Protein Complexes for Structure Determination. *ACS Pharmacol Transl Sci* **1**, 12-20, doi:10.1021/acsptsci.8b00017 (2018).

3 Maeda, S. *et al.* Development of an antibody fragment that stabilizes GPCR/G-protein complexes. *Nature Communications* **9**, doi:ARTN 3712 10.1038/s41467-018-06002-w (2018).

4 Zhuang, Y. *et al.* Structural insights into the human D1 and D2 dopamine receptor signaling complexes. *Cell* **184**, 931-942. e918 (2021).

5 Xu, P. *et al.* Structures of the human dopamine D3 receptor-Gi complexes. *Molecular Cell* (2021).

6 Zheng, S. Q. *et al.* MotionCor2: anisotropic correction of beam-induced motion for improved cryo-electron microscopy. *Nat Methods* **14**, 331-332, doi:10.1038/nmeth.4193 (2017).

7 Zhang, K. Gctf: Real-time CTF determination and correction. *J Struct Biol* **193**, 1-12, doi:10.1016/j.jsb.2015.11.003 (2016).

8 Scheres, S. H. W. RELION: Implementation of a Bayesian approach to cryo-EM structure determination. *J Struct Biol* **180**, 519-530, doi:10.1016/j.jsb.2012.09.006 (2012).

9 Kato, H. E. *et al.* Conformational transitions of a neurotensin receptor 1-Gi1 complex. *Nature*, doi:10.1038/s41586-019-1337-6 (2019).

10 Sanchez-Garcia, R. *et al.* DeepEMhancer: a deep learning solution for cryo-EM volume post-processing. *bioRxiv* (2020).

11 Pettersen, E. F. *et al.* UCSF Chimera--a visualization system for exploratory research and analysis. *J Comput Chem* **25**, 1605-1612, doi:10.1002/jcc.20084 (2004).

12 Emsley, P. & Cowtan, K. Coot: model-building tools for molecular graphics. *Acta Crystallogr D Biol Crystallogr* **60**, 2126-2132, doi:10.1107/S0907444904019158 (2004).

13 Croll, T. I. ISOLDE: a physically realistic environment for model building into low-resolution electron-density maps. *Acta Crystallogr D Struct Biol* **74**, 519-530, doi:10.1107/S2059798318002425 (2018).

14 Adams, P. D. *et al.* PHENIX: a comprehensive Python-based system for macromolecular structure solution. *Acta Crystallogr D Biol Crystallogr* **66**, 213-221, doi:10.1107/S0907444909052925 (2010).

15 Chen, V. B. *et al.* MolProbity: all-atom structure validation for macromolecular crystallography. *Acta Crystallogr D* **66**, 12-21, doi:10.1107/S0907444909042073 (2010).

16 Pettersen, E. F. *et al.* UCSF ChimeraX: Structure visualization for researchers, educators, and developers. *Protein Sci*, doi:10.1002/pro.3943 (2020).

Fig. 1

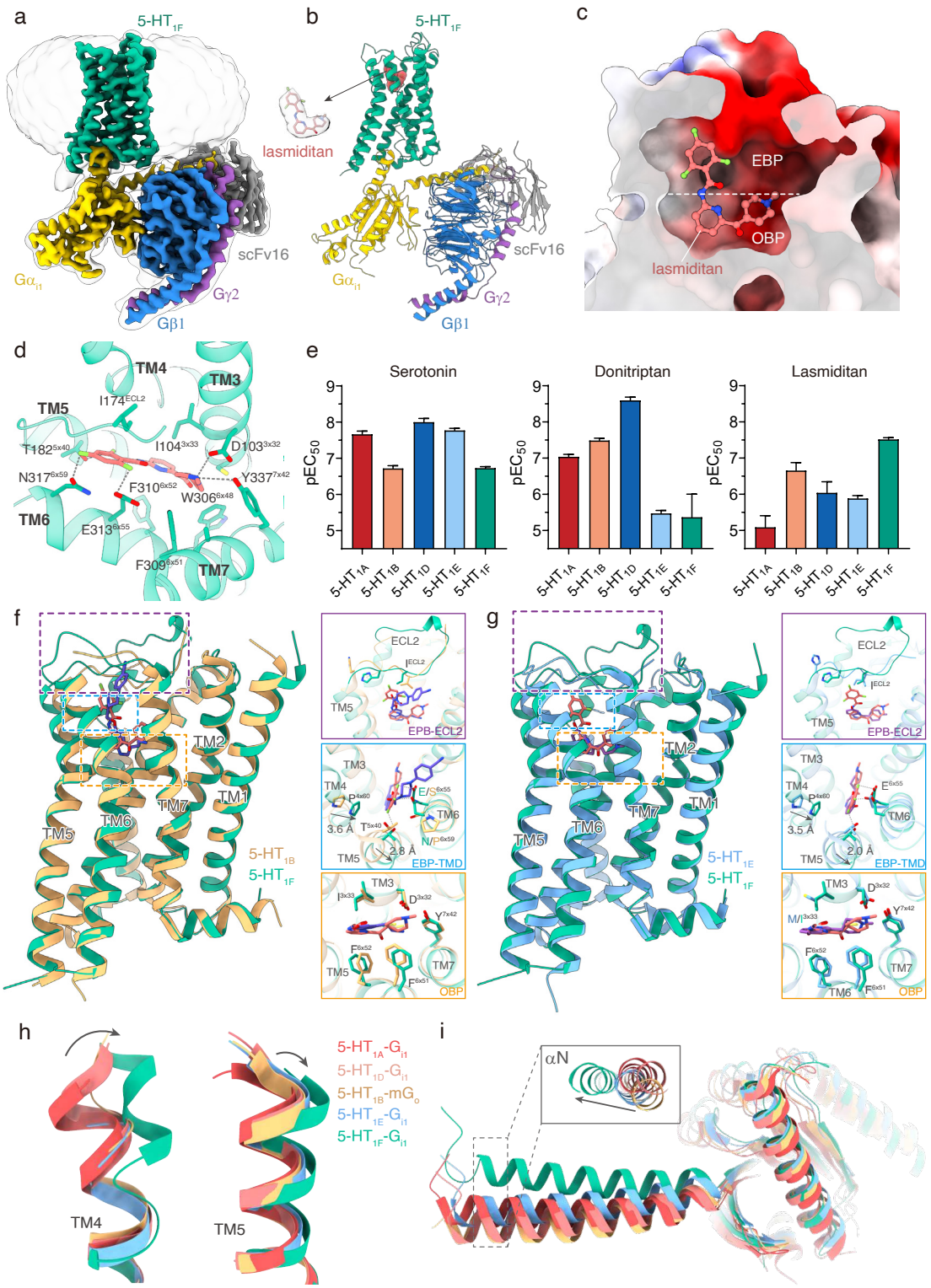

Fig. S1

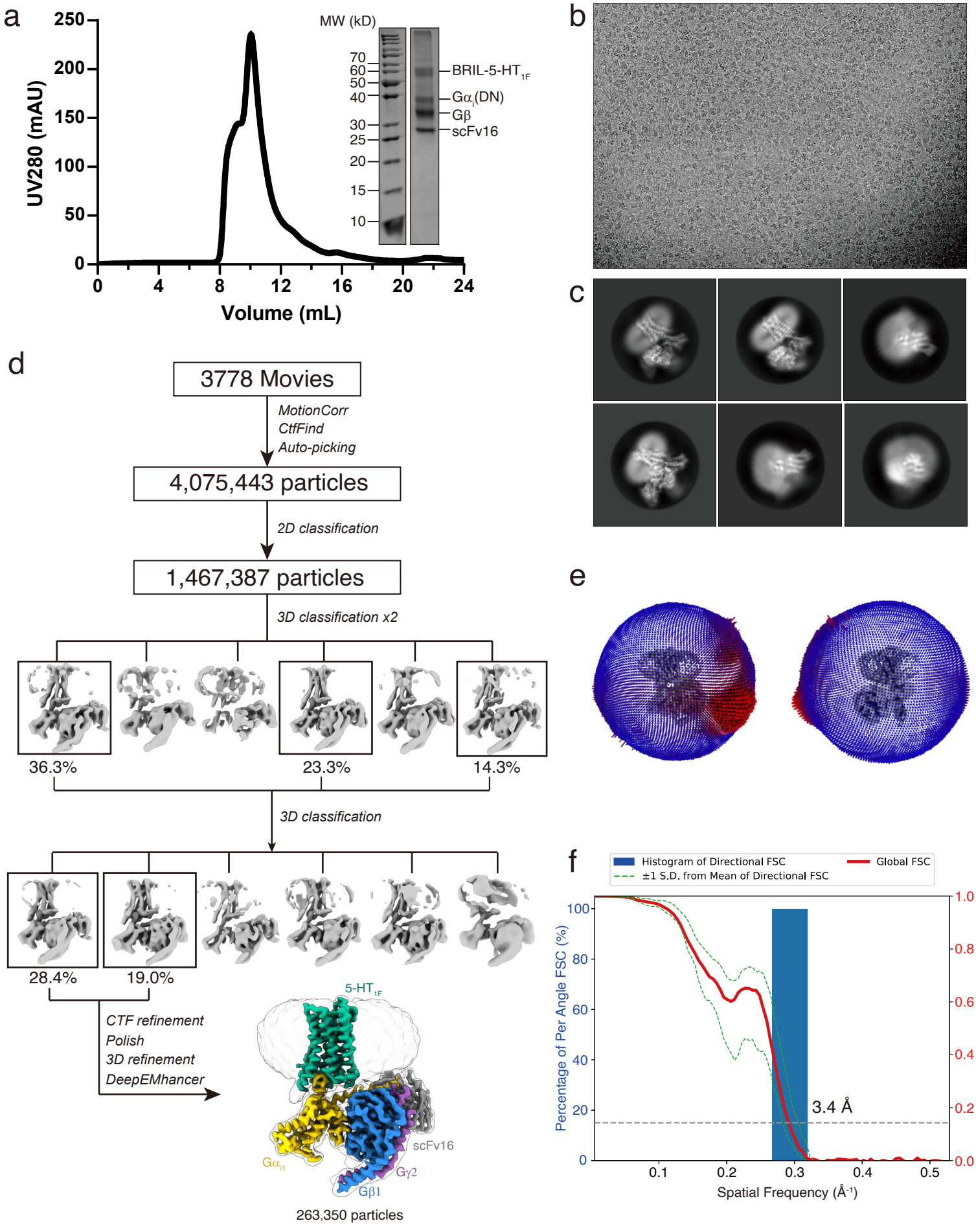

Fig. S2

a

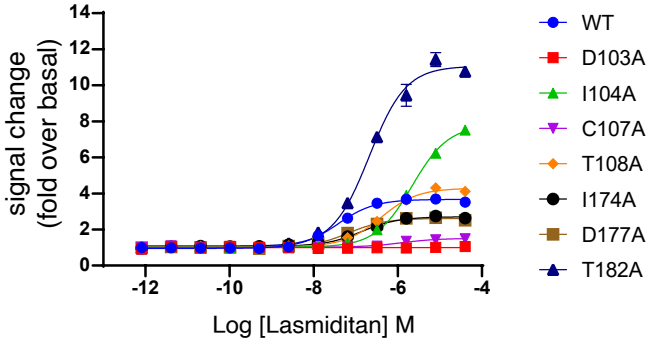

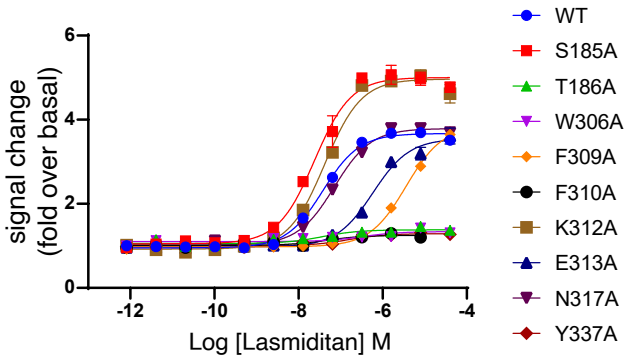

b

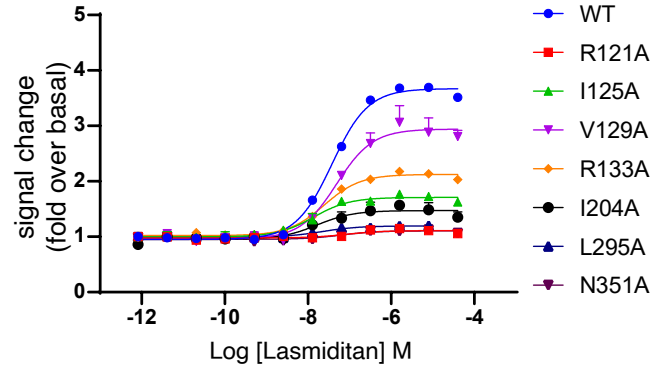

c

Const.	pEC50	ΔpEC50
R121A	7.07 ± 0.31	-0.35
I125A	7.86 ± 0.13	0.44
V129A	7.31 ± 0.10	-0.11
R133A	7.61 ± 0.06	0.19
I204A	7.78 ± 0.29	0.36
R287A	7.15 ± 0.05	-0.27
L295A	7.65 ± 0.15	0.23
N351A	7.20 ± 0.34	-0.22
ECL2(1A)	< 4.0	< -3.42
ECL2(1B)	< 4.0	< -3.42
ECL2(1D)	< 4.0	< -3.42
ECL2(1E)	< 4.0	< -3.42

d

Const.	pEC50	ΔpEC50
WT	7.42 ± 0.03	0
D103A	< 4.0	< -3.42
I104A	5.66 ± 0.01	-1.76
C107A	5.91 ± 0.12	-1.5
T108A	6.40 ± 0.03	-1.02
T182A	6.67 ± 0.04	-0.74
S185A	7.62 ± 0.06	0.2
T186A	7.43 ± 0.29	0.01
W306A	< 4.0	< -3.42
F309A	5.44 ± 0.02	-1.98
F310A	< 4.0	< -3.42
K312A	7.38 ± 0.05	-0.04
E313A	6.23 ± 0.06	-1.19
N317A	7.15 ± 0.03	-0.27
Y337A	< 4.0	< -3.42
I174A	6.86 ± 0.04	-0.56
D177A	7.17 ± 0.04	-0.25

Fig. S3

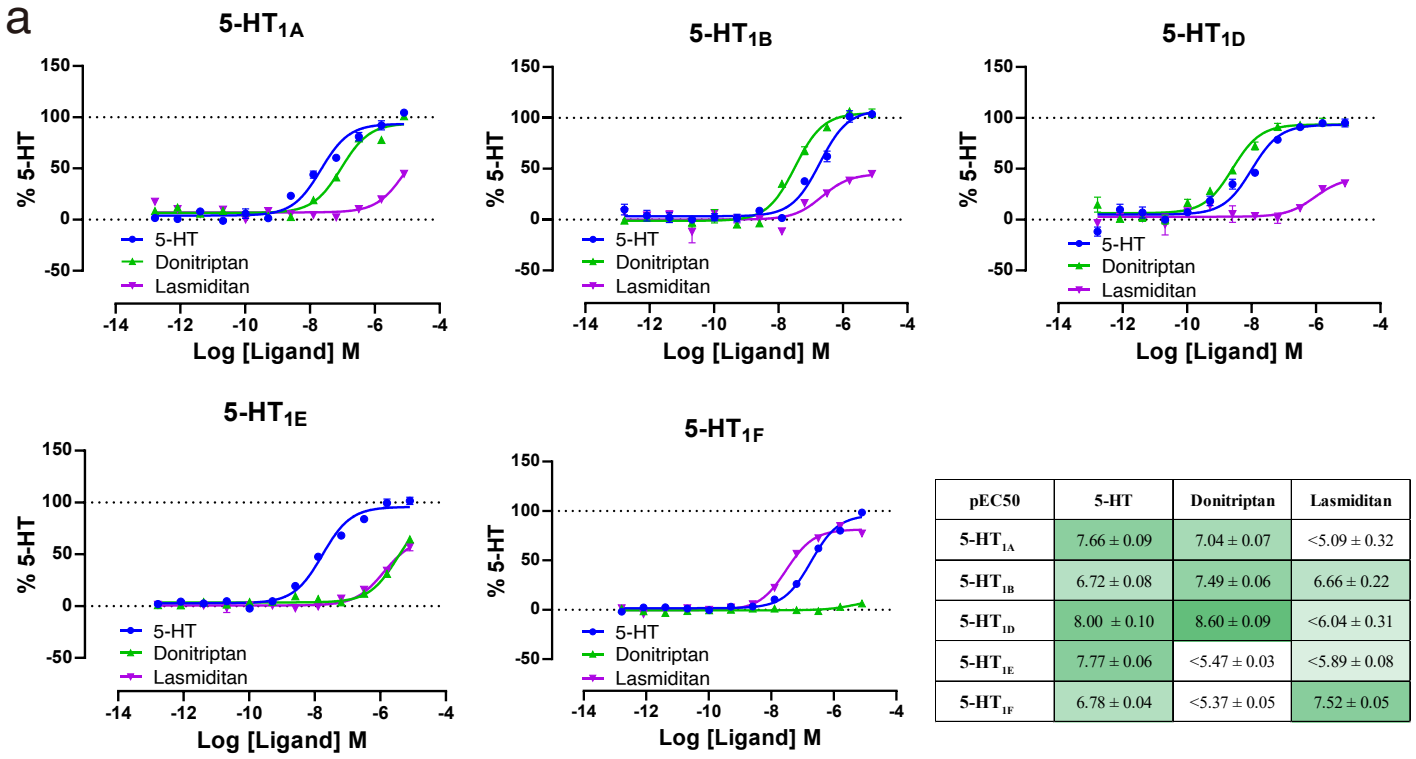

pEC50	5-HT	Donitriptan	Lasmiditan
5-HT$_{1A}$	7.66 ± 0.09	7.04 ± 0.07	<5.09 ± 0.32
5-HT$_{1B}$	6.72 ± 0.08	7.49 ± 0.06	6.66 ± 0.22
5-HT$_{1D}$	8.00 ± 0.10	8.60 ± 0.09	<6.04 ± 0.31
5-HT$_{1E}$	7.77 ± 0.06	<5.47 ± 0.03	<5.89 ± 0.08
5-HT$_{1F}$	6.78 ± 0.04	<5.37 ± 0.05	7.52 ± 0.05

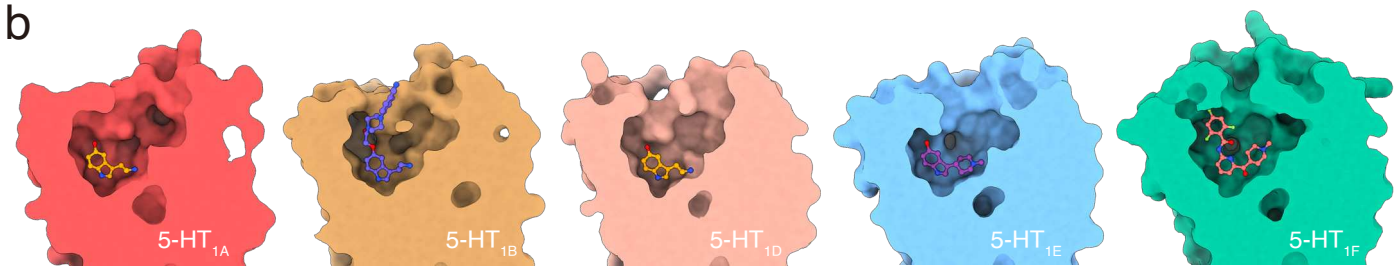

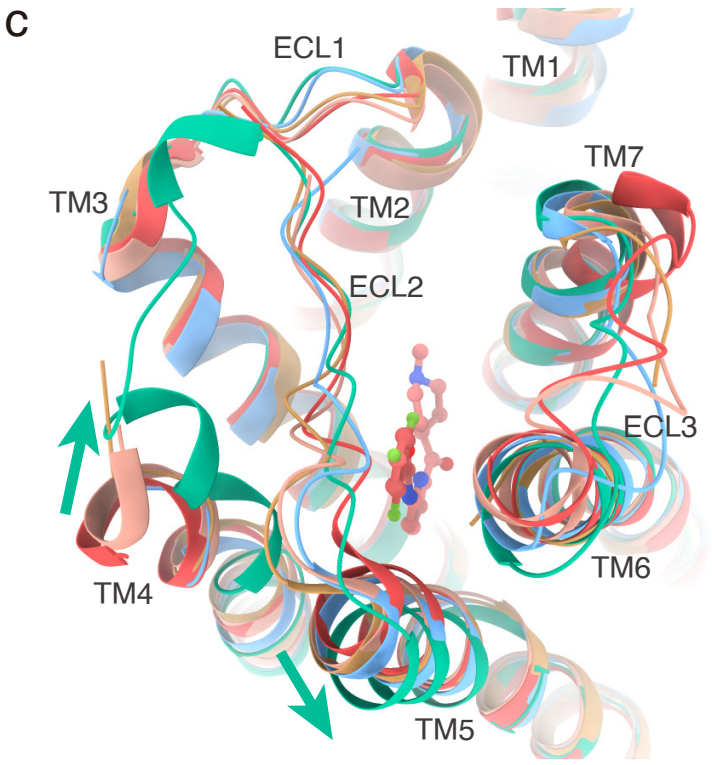

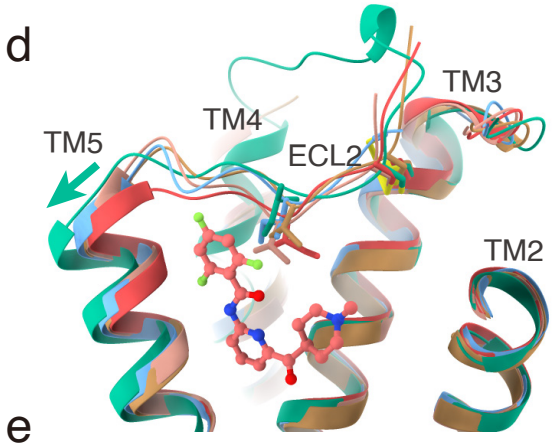

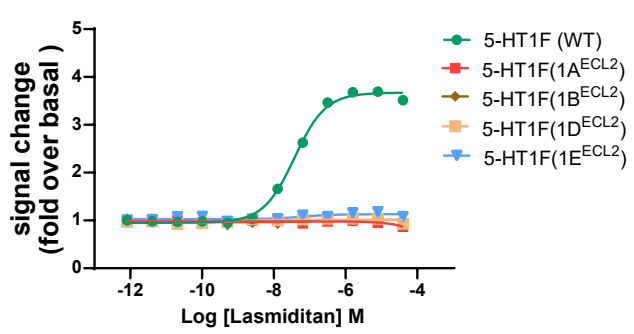

Fig. S4